ADVANCED FUNCTIONAL MATERIALS

# Supporting Information

for *Adv. Funct. Mater.,* DOI: 10.1002/adfm.201806997

# Exciton Dynamics and Effects of Structural Order in Morphology-Controlled J-Aggregate Assemblies

*Surendra B. Anantharaman, Thilo Stöferle, Frank A. Nüesch, Rainer F. Mahrt,* and Jakob Heier**

# Supporting Information

## Exciton dynamics and effects of structural order in morphology-controlled J-aggregate assemblies

Surendra B. Anantharaman, Thilo Stöferle, Frank A. Nüesch, Rainer F. Mahrt,* and Jakob Heier*

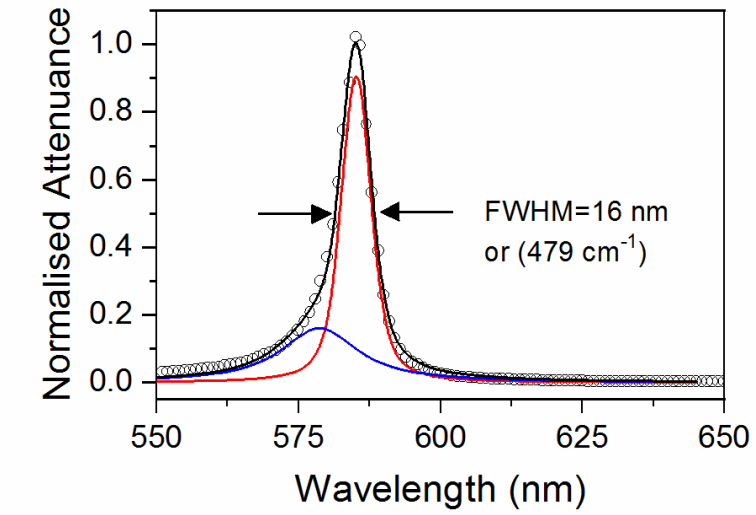


**Figure S1.** The normalized attenuance of the J-aggregate peak measured from dye dissolved in water was de-convoluted to determine the full-width at half-maximum (FWHM). The measured J-aggregate peak is shown as scatter points, which is de-convoluted into two peaks – main J-aggregate peak as red line and the contribution from uncoupled molecules as blue line. The fitted J-aggregate curve is represented as black line.

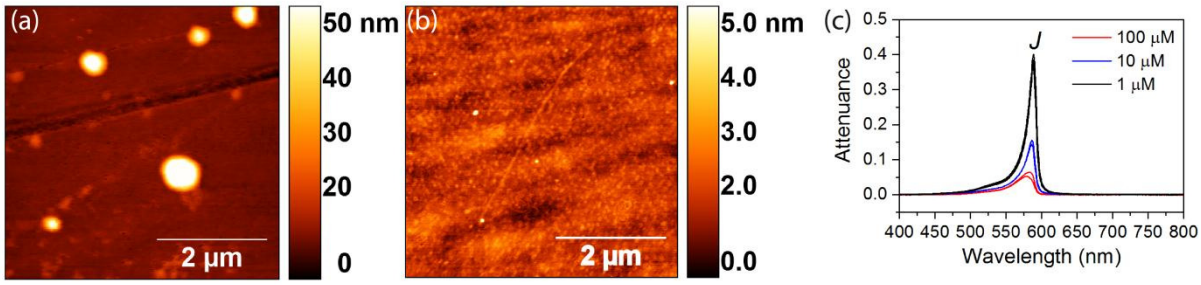


**Figure S2.** PAMAM deposited on glass substrates at (a) high concentration (100 µM) and (b) low concentration (1 µM), forming PAMAM aggregates and a PAMAM monolayer, respectively. The J-aggregates are deposited on glass substrates functionalised with different PAMAM concentration. (c) The attenuance shows strong absorption from J-aggregate films deposited on the PAMAM monolayer. The spectra acquired at multiple spots from the sample are shown overlayed in same colour.

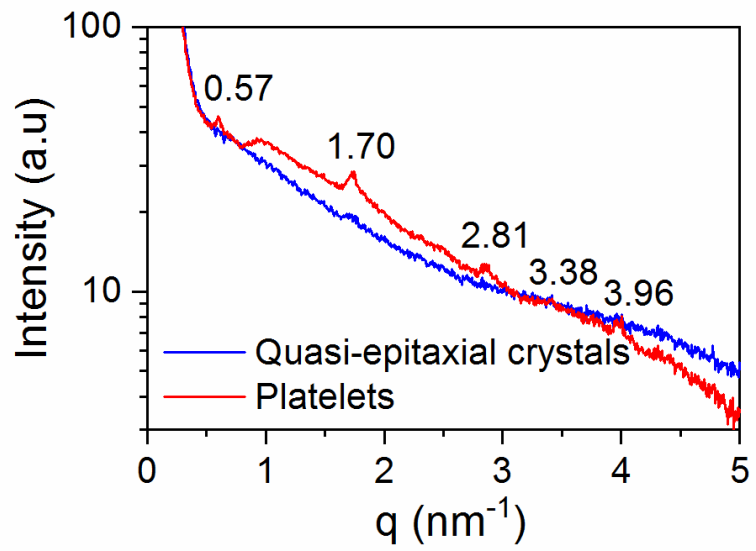


**Figure S3.** Synchrotron SAXS measurement for platelets and quasi-epitaxial crystal thin films.

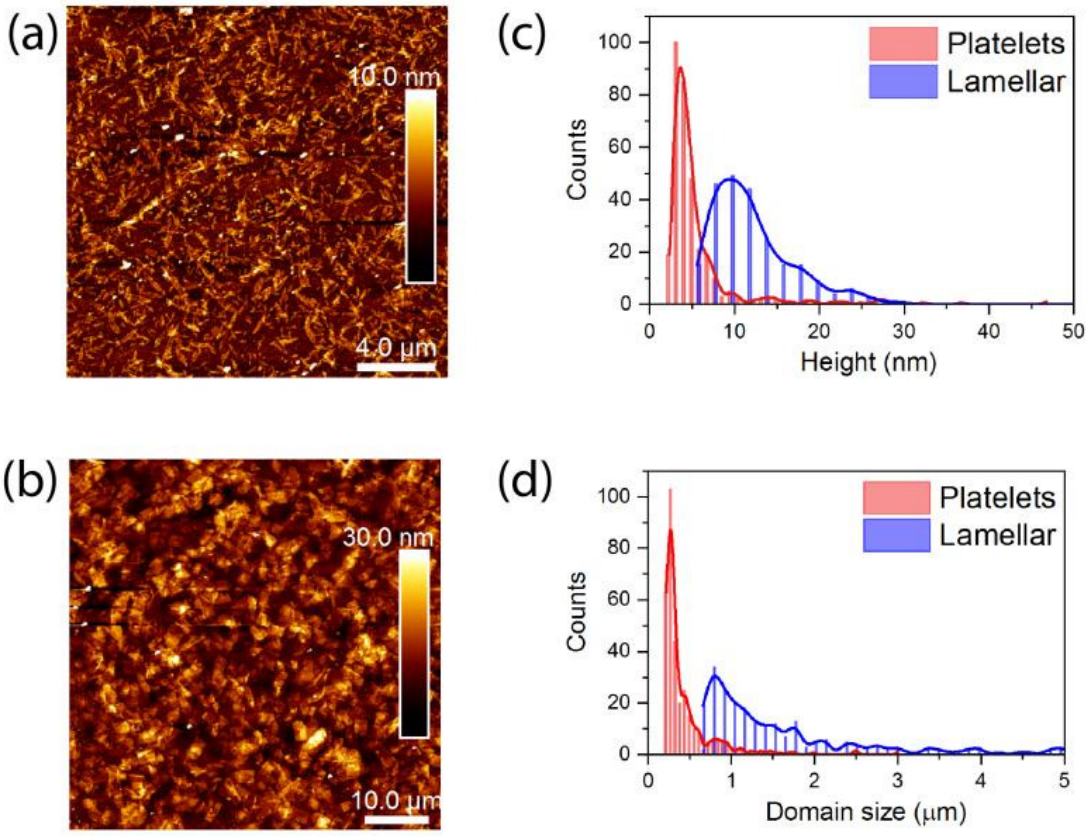


**Figure S4.** Topographical image of platelets (a) and lamellar films (b) with their corresponding height (c) and domain size (d) distributions. The thickness of the platelets and lamellar films are ~ 4nm and 10 nm, respectively as shown in (c).

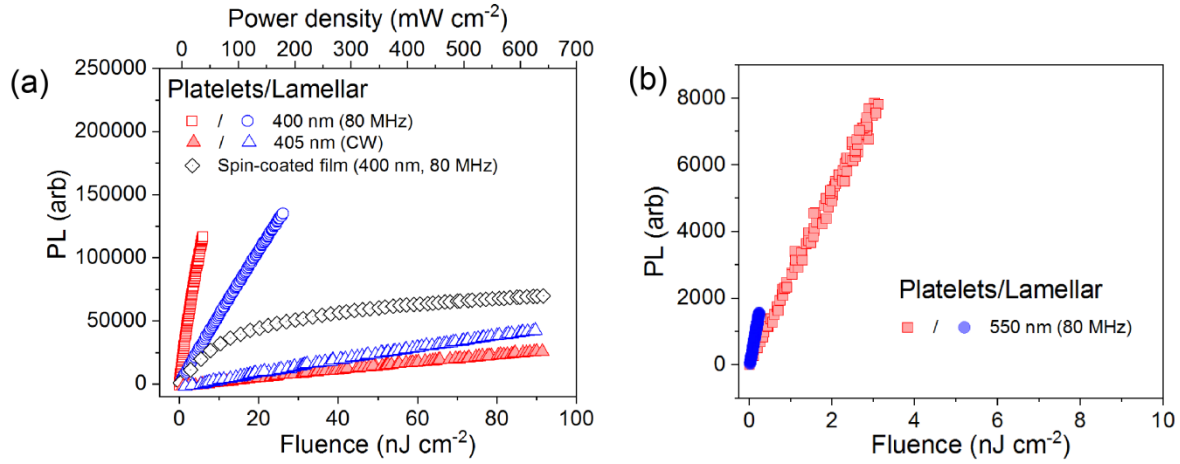


**Figure S5.** Integrated PL intensity versus fluence acquired for continuous-wave and pulsed ultrafast excitation at 400 nm (a) and 550 nm (b) for platelets and lamellar films at 6 K. For comparison, spin-coated films were studied with ultrafast excitation at 400 nm, 80 MHz at 6 K.

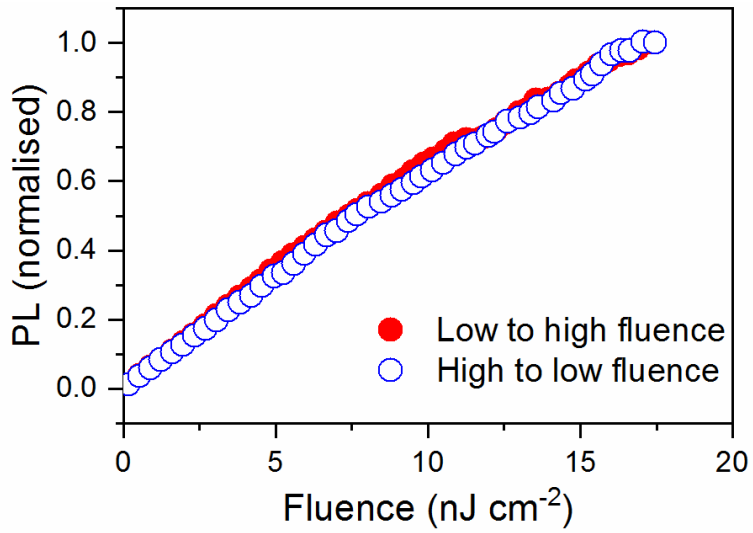


**Figure S6.** Normalised PL versus fluence for platelets excited at 400 nm, 80 MHz at 6 K from low to high fluence and vice-versa to demonstrate reversibility of the process. From a power-law fit we obtain an exponent of 0.77 for both curves.

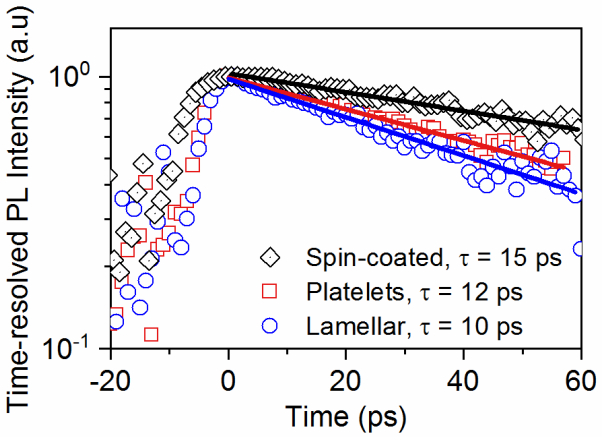


**Figure S7.** Time-resolved spectrally-integrated dynamics (fluence of 26 nJ $cm^{-2}$) with the lines representing the fits of an exponential decay to the data between 0 and 60 ps.

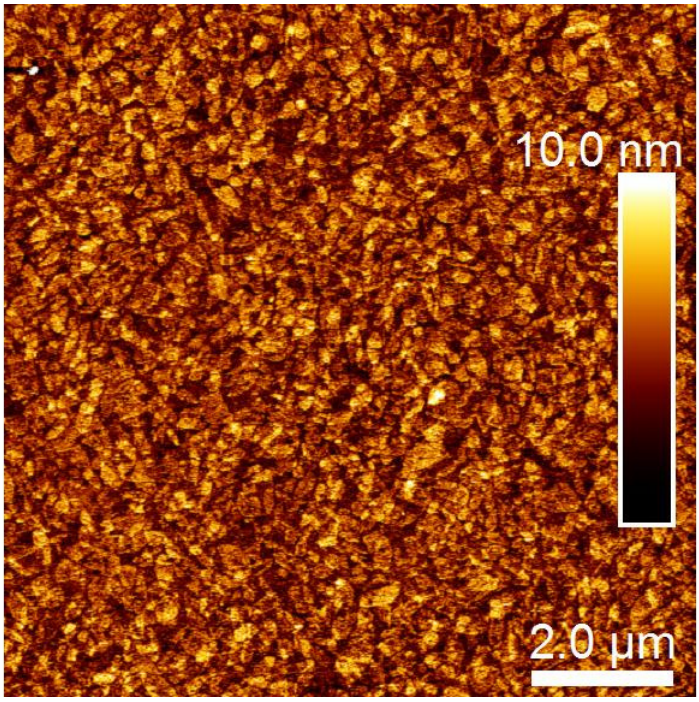


**Figure S8.** Topography of spin-coated film obtained from J-aggregate dye solution (5 wt% dye) in water.

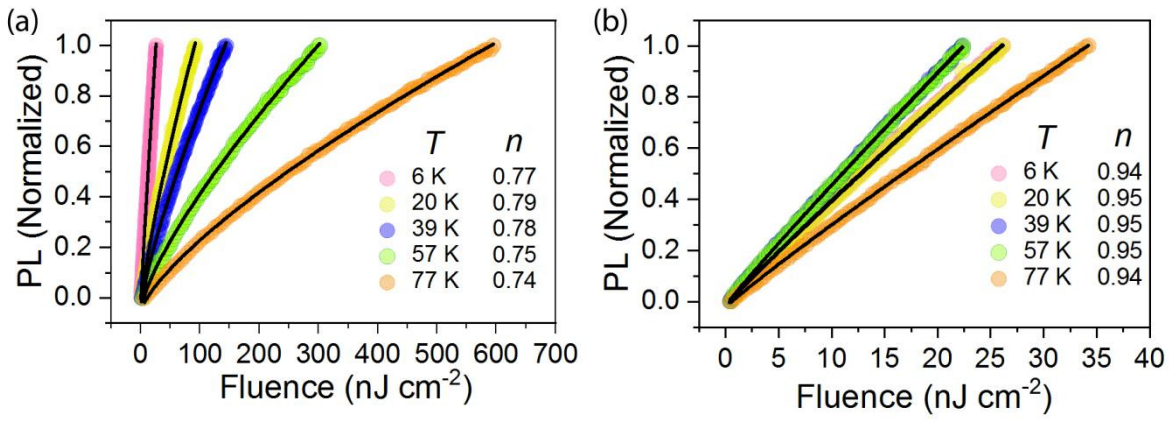


**Figure S9.** PL intensity vs. fluence recorded at different temperatures for (a) platelets and (b) lamellar films, keeping the excitation wavelength at 400 nm. The respective exponents n from power-law fits to the data are shown in the legend. It should be noted that, at 77 K, an enormous amount of pump power is required for acquiring PL in platelets (~500 nJ $cm^{-2}$), unlike lamellar films (< 50 nJ $cm^{-2}$).

## S1. Charge generation and recombination time for excitation at 400 nm

In the following, the conditions for charge carrier build-up at 400 nm excitation are estimated. Furthermore, we show that the distance between two charges is much farther (715 nm) than the film thickness (~5 nm) of the J-aggregates used in this study. This implies the 2D recombination is a more appropriate model than 3D. In the simplest approach, the charge carrier density is given by the charge generation rate G(λ,T,I) and a bimolecular recombination rate R(N,T), where λ is the photon wavelength, T the temperature, I the fluence and N the two-dimensional carrier density:[1]

$$\frac{dN}{dt} = G(\lambda, T, I) - R(N, T) \qquad (S1)$$

$$\frac{dN}{dt} = G_0(\lambda, T, I) \cdot \eta - N / \tau \quad \text{(S2)}$$

Here, $G_0$ is the photon flux averaged over time, $\eta$ is the efficiency of the charge generation, and $\tau$ is the carrier recombination time, which is given by

$$\tau = \frac{8\varepsilon_0 \varepsilon}{15\sqrt{\pi} e \mu} N^{-3/2} \quad \text{(S3)}$$

In our experiment (we consider a large number of pulses), $G_0$' (= $1.60 \cdot 10^{23}$ $s^{-1}$ $m^{-2}$) measured with a power meter needs to be multiplied by the absorbance (= 0.003 ± 0.001) to yield the effective absorbed photon flux: $G_0 = 5.248 \pm 1.89 \cdot 10^{20}$ $s^{-1}$ $m^{-2}$. $\eta$ can be assumed to be rather large, otherwise charge-exciton quenching would not be able to compete with the major non-radiative process in the system: we assumed $\eta := 0.5$ in the following calculation. Furthermore, the relative dielectric constant ε = 4 is used. For well-ordered lamellar films, the carrier mobility can reach $10^{-3}$ $m^2 V^{-1} s^{-1}$ (= 10 $cm^2 V^{-1} s^{-1}$). At equilibrium, dN/dt = 0, which enables to calculate the equilibrium charge density:

$$G_0 \cdot \eta - \frac{N}{\tau} = 0 \quad \text{(S4)}$$

Substituting Equation (S3) in Equation (S4) gives,

$$N^{5/2} = \frac{8\varepsilon_0 \varepsilon G_0 \eta}{15\sqrt{\pi} e \mu}$$

$$N^{5/2} = \frac{8 \times 8.854 \times 10^{-12} C V^{-1} m^{-1} \times 4 \times (5.248 \pm 1.89) \times 10^{20} s^{-1} m^{-2} \times 0.5}{15\sqrt{\pi} \times 1.602 \times 10^{-19} C \times 10^{-3} m^2 V^{-1} s^{-1}}$$

$$N^{5/2} = 1.7 \pm 0.6 \cdot 10^{31} m^{-5}$$

$$N = 3.1 \pm 2.1 \cdot 10^{12} m^{-2}$$

In other words, the average distance between charge carriers would be about 564 nm, which is much larger than the platelet size and roughly the size of lamellar crystals. As static disorder is increased in the system, the mobility may be much lower than the highest mobility observed in 3D molecular crystals.[2] Based on the above estimation, we infer that in such a bulk carrier quenching model, charge carriers would have to be trapped more severely in order to account for charge – exciton quenching in platelets or spin coated films (corresponding to charge carrier mobilities of about $10^{-8}$ to $10^{-6}$ $cm^2$ $V^{-1}$ $s^{-1}$ at low temperature). Following this argument to the end, the charge carrier mobility of $10^{-6}$ $cm^2$ $V^{-1}$ $s^{-1}$ would imply a carrier lifetime of $\tau = 15$ μs and a two-dimensional diffusion length of $L_D = 2 \cdot \sqrt{D \cdot \tau} = 2 \cdot \sqrt{\frac{\mu k T \tau}{e}} = 1.8\text{nm}$, conforming to long-lived charges that are closely localized near their generation sites.

**Table S1.** Full-width at half-maximum (FWHM) of the photoluminescence spectrum collected as a function of temperature for platelets and lamellar films.

| **Temperature (K)** | **Platelets** | | | **Lamellar** | | |
|---|---|---|---|---|---|---|
| | Gaussian width ($cm^{-1}$) | Lorentzian width ($cm^{-1}$) | FWHM ($cm^{-1}$) | Gaussian width ($cm^{-1}$) | Lorentzian width ($cm^{-1}$) | FWHM ($cm^{-1}$) |
| 6 | 100.27 ± 3.83 | 92.33 ± 3.69 | 158.45 ± 1.45 | 58.64 ± 2.58 | 75.78 ± 2.12 | 108.94 ± 0.95 |
| 20 | 100.27 | 91.07 ± 2.04 | 157.55 ± 1.46 | 58.64 | 78.61 ± 0.90 | 111.14 ± 0.71 |
| 39 | 100.27 | 103.27 ± 2.54 | 166.41 ± 1.87 | 58.64 | 91.91± 0.90 | 121.72 ± 0.73 |
| 57 | 100.27 | 116.52 ± 3.74 | 176.29 ± 2.83 | 58.64 | 102.01 ± 0.82 | 129.99 ± 0.68 |
| 77 | 100.27 | 151.83 ± 5.54 | 203.84 ± 4.45 | 58.64 | 115.58 ± 0.81 | 141.37 ± 0.69 |
| 100 | 100.27 | 164.51 ± 5.75 | 214.11 ± 4.70 | 58.64 | 128.23 ± 0.81 | 152.22 ± 0.70 |

**Table S2.** Lifetime of the singlet exciton in platelets and lamellar films measured at 6 K for different laser fluence.

| Laser fluence ($nJ\ cm^{-2}$) | 400 nm, 80 MHz | | Laser fluence ($mJ\ cm^{-2}$) | 505 nm, 1 kHz | |
|---|---|---|---|---|---|
| | Platelets (ps) | Lamellar (ps) | | Platelets (ps) | Lamellar (ps) |
| 26 | 11.7 | 9.8 | 2.08 | 43 | 39.5 |
| 52 | 10.6 | 8.8 | 4.15 | 50 | 61.4 |
| 78 | 10.1 | 8 | 6.24 | 51.7 | 71.4 |

**References:**

[1] A. V. Nenashev, F. Jansson, S. D. Baranovskii, R. Österbacka, A. V. Dvurechenskii, F. Gebhard, Applied Physics Letters **2010**, 96, 213304.

[2] G. Schweicher, Y. Olivier, V. Lemaur, Y. H. Geerts, Israel Journal of Chemistry **2014**, 54, 595.